Appl. Math. Mech. -Engl. Ed., **42**(6), 755–770 (2021)

APPLIED MATHEMATICS AND MECHANICS (ENGLISH EDITION)

https://doi.org/10.1007/s10483-021-2741-8

Design and dynamic analysis of integrated architecture for vibration energy harvesting including piezoelectric frame and mechanical amplifier*

Xiangjian DUAN[1], Dongxing CAO[2,3,†], Xiaoguang LI[2,3], Yongjun SHEN[4]

1. Beijing Institute of Structure and Environment Engineering, Beijing 100076, China;
2. Faculty of Materials and Manufacturing, Beijing University of Technology, Beijing 100124, China;
3. Beijing Key Laboratory of Nonlinear Vibrations and Strength of Mechanical Structures, Beijing 100124, China;
4. State Key Laboratory of Mechanical Behavior and System Safety of Traffic Engineering Structures, Shijiazhuang Tiedao University, Shijiazhuang 050043, China

(Received Apr. 1, 2021 / Revised Apr. 15, 2021)

Abstract Vibration energy harvesters (VEHs) can transform ambient vibration energy to electricity and have been widely investigated as promising self-powered devices for wireless sensor networks, wearable sensors, and applications of a micro-electro-mechanical system (MEMS). However, the ambient vibration is always too weak to hinder the high energy conversion efficiency. In this paper, the integrated frame composed of piezoelectric beams and mechanical amplifiers is proposed to improve the energy conversion efficiency of a VEH. First, the initial structures of a piezoelectric frame (PF) and an amplification frame (AF) are designed. The dynamic model is then established to analyze the influence of key structural parameters on the mechanical amplification factor. Finite element simulation is conducted to study the energy harvesting performance, where the stiffness characteristics and power output in the cases of series and parallel load resistance are discussed in detail. Furthermore, piezoelectric beams with variable cross-sections are introduced to optimize and improve the energy harvesting efficiency. Advantages of the PF with the AF are illustrated by comparison with conventional piezoelectric cantilever beams. The results show that the proposed integrated VEH has a good mechanical amplification capability and is more suitable for low-frequency vibration conditions.

Key words vibration energy harvesting, mechanical amplifier, piezoelectric frame (PF), amplification frame (AF), variable cross-section beam

* Citation: DUAN, X. J., CAO, D. X., LI, X. G., and SHEN, Y. J. Design and dynamic analysis of integrated architecture for vibration energy harvesting including piezoelectric frame and mechanical amplifier. *Applied Mathematics and Mechanics* (*English Edition*), **42**(6), 755–770 (2021) https://doi.org/10.1007/s10483-021-2741-8

† Corresponding author, E-mail: caostar@bjut.edu.cn

Project supported by the National Natural Science Foundation of China (Nos. 11972051 and 11672008) and the Opening Project Foundation of the State Key Laboratory of Mechanical Behavior and System Safety of Traffic Engineering Structures (No. KF-2020-11)

©The Author(s) 2021

Chinese Library Classification O326
2010 Mathematics Subject Classification 70J35

1 Introduction

Vibration is a ubiquitous phenomenon in daily life and industrial production. In recent years, many researchers have tried to scavenge vibration energy for micro-power generation, which can be applied to low-power electrical devices such as wireless sensors and detectors[1–4]. The conversion principles for the vibration energy harvesting mainly include the electrostatic principle[5–7], the piezoelectric principle[8–15], the electromagnetic principle[16–18], and the ferroelectric material[19–22]. The piezoelectric vibration energy harvesting technique has received much attention because of its advantages of high energy density, fast response speed, and simple structure.

The most commonly used structures for the vibration energy harvester (VEH) are cantilever piezoelectric beams and plates. The critical challenge for such energy harvesters lies in the limited power output due to the lower energy conversion efficiency of the structures. To increase the output power density, one promising solution is the introduction of a force amplifier, which can amplify displacements or forces and increase the load capacity of the transducer. Piezoelectric energy harvesters with mechanical amplifiers have received extensive attention from many scholars. Kim et al.[23–24] modeled a power generation from the cymbal transducer and developed the theory for the Belleville spring earlier. Li et al.[25] designed a flex-compressive-mode piezoelectric transducer with a cymbal for mechanical vibration energy harvesting. Mo et al.[26] proposed a unimorph lead zirconate titanate cymbal harvester to sustain higher mechanical loads by replacing the lead zirconate titanate monolayer with the lead zirconate titanate/steel composite between metals end caps. Moure et al.[27] embedded a piezoelectric cymbal on the road to scavenge the wasted and unused vibrational energy from the rolling of the car. Wang et al.[28] designed a flex-compressive piezoelectric energy harvesting cell with a large load capacity, and the force transfer coefficient can be adjusted. Zhao et al.[29] designed a cymbal for harvesting energy from asphalt pavements. Ling et al.[30] proposed an attenuated displacement amplification of multistage compliant mechanisms. Cao et al.[31] designed an analytical model to describe the static displacement and force interactions between generic serial-parallel compliant mechanisms and piezo-stacks. Evans et al.[32] investigated a force-amplified piezoelectric stack device that was found to have a maximum level of amplification at a low-frequency level. Multi-stage force amplification frames (AFs) were proposed in Refs. [33]–[35] to achieve high power output for piezoelectric stack-based energy harvesters. Cao et al.[36] designed a piezoelectric stack energy harvester with a force amplifier to scavenge the vibration energy of pressure fluctuations in pipeline systems.

Prior studies show that various types of structures can be used as force AFs, such as cymbal structures and compliant mechanisms. The working principle of all amplifiers is the mutual conversion between forces and displacements. In this paper, the frame composed of piezoelectric beams and a mechanical amplifier is proposed for vibration energy harvesting, where a piezoelectric frame (PF) composed of multiple piezoelectric beams and an AF composed of a link mechanism are designed. The proposed VEH can easily achieve resonance conditions for low frequency excitations.

The rest of the paper is organized as follows. In Section 2, the integrated structure of the harvester is introduced, and the mechanical amplification factor is analyzed. In Section 3, the dynamic analysis of the harvester is studied theoretically. In Section 4, the harvesting performance is discussed in detail based on the finite element analysis. Finally, the conclusions are summarized.

2 Structure design

Figure 1 shows the schematic diagram of the proposed VEH, where the PF (see Fig. 1(b)) and the AF (see Fig. 1(c)) are two main components of integrated architectures. Piezoelectric sheets are adhered at the position where the strain is relatively concentrated during the PF deformation to improve its conversion efficiency. The structure design of double rotating beams in the AF ensures that the holding part will not twist during the operating status. The sliding pair moves up and down along the rail to bend the piezoelectric sheets pasted on the PF. The strain distributions of the PF and the PF with the AF are shown in Fig. 2, respectively. The strain on the PF mainly appears in the fixed place. Therefore, piezoelectric sheets should be pasted in the fixed place. Up to eight piezoelectric sheets can be attached to one PF. The strain distribution for each piezoelectric sheet in the PF is almost identical.

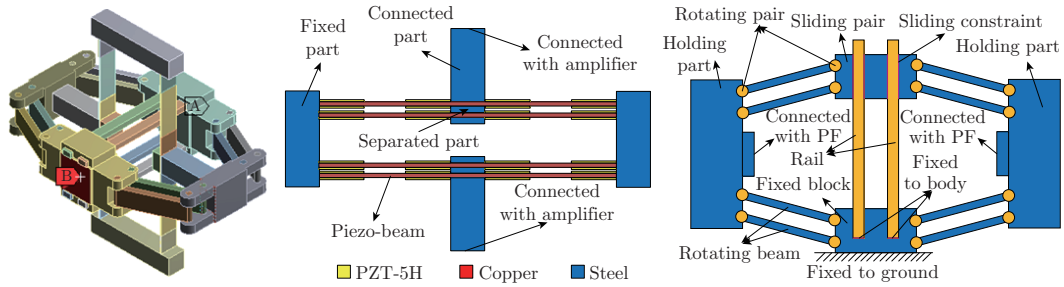

(a) Three-dimensional model (b) PF (c) AF

Fig. 1 Schematic diagrams of proposed VEH (color online)

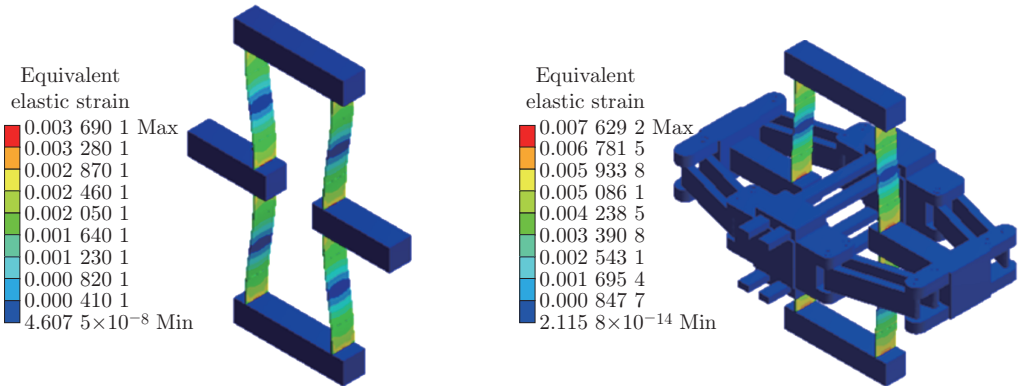

(a) PF (b) PF with AF

Fig. 2 Strain distributions of energy harvester under static pressure (color online)

The conventional harvester structures are mostly cantilever beams with one end fixed and the other end free. Here, the integrated architecture has four fixed ends of the piezo-beam in the PF, making the strain concentrated in multiple locations during vibration. This means that the utilization rate of piezoelectric materials will be higher than that of single piezoelectric cantilever beams.

Except that the piezo-beams in the PF are elastic, the rest of the energy harvester is considered to be rigid. Due to the symmetry of the structure, the simplified dynamic model of the PF with the AF is shown in Fig. 3, where k is the stiffness of the PF when the piezoelectric

beams are deformed. In the model, m_1, m_2, and m_3 are the masses of the sliding pair, the holding part, and the connected part, respectively. The lengths of the rotating beams and the connected part are denoted by a and b, respectively. The angle between the rotating beam and the horizontal plane is represented by θ.

The allowable motion range of the sliding pair is

$$0 < y_1 < 2a \sin\theta, \tag{1}$$

where y_1 represents the displacement of m_1 along the y-direction.

The tensile displacement of the PF determines the bending stress on the piezoelectric sheet. Based on the geometric relationship, the maximum tensile displacement of the PF is

$$s_{\max} = a - b. \tag{2}$$

To ensure that the deformation of the piezoelectric sheet is in the elastic stage, the bending stress should be less than the bending yield strength of the material (450 MPa). The finite element simulation is used for the static analysis of the PF with the AF. As shown in Fig. 4, when the PF reaches the maximum tensile displacement, the bending strain distribution on the piezoelectric sheet meets the requirements of working conditions. The key parameters are shown in Table 1. Of course, the reasonable structure parameters must be designed to avoid the damage of the PF.

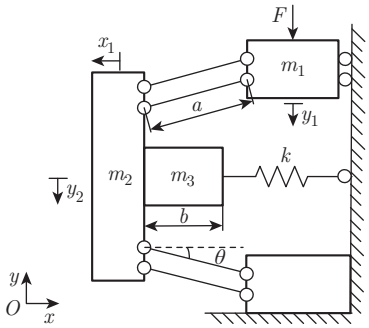

Fig. 3 Simplified dynamic model of PF with AF

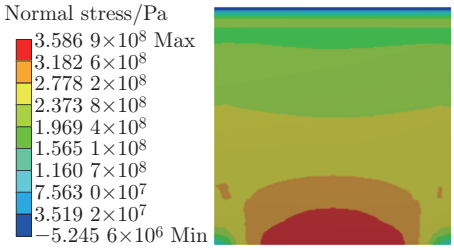

Fig. 4 Strain distributions on piezoelectric sheets under maximum tensile displacement of PF (color online)

Table 1 Key parameters of PF with AF

Parameter	Value	Parameter	Value
Length of rotating beam a/mm	35	Mass of connected part m_3/kg	0.042
Length of connected part b/mm	28	Piezoelectric constant d_{31}	-2.74×10^{-10}
Dielectric constant $\varepsilon_{33}^{\mathrm{T}}$	$3\,100 \times 8.854 \times 10^{-12}$	Structural angle θ/rad	0.44
Length of piezo-beam L/mm	100	Area of piezoelectric sheet A_3/mm^2	1×10^{-4}
Mass of sliding pair m_1/kg	0.064	Thickness of piezoelectric sheet d_3/mm	1×10^{-4}
Mass of holding part m_2/kg	0.048		

The static analysis of the PF with the AF can be conducted with Newton's method,

$$F_{\mathrm{in}} \cot\theta = 2F \cot\theta = ks, \tag{3}$$

where F_{in} is the force acting on the sliding pair. s is the displacement of the PF. k is the stiffness of the PF.

The ratio of the force acting on the PF to the external force is defined as the mechanical amplification factor β, i.e.,

$$\beta = \frac{|ks|}{|F_{\text{in}}|}, \tag{4}$$

where $|ks|$ is the amplitude of the force acting on the PF, and $|F_{\text{in}}|$ is the amplitude of the force acting on the sliding pair.

According to the principle of the mechanical amplifier, the amplification factor will sensibly reflect the effect of the AF on energy harvesting. As shown in the table in Section 4, $\beta = \cot\theta$ is constant (θ is the angle after deformation) under static force. For dynamic conditions, the mechanical amplification factor will be further discussed in the next section.

3 Dynamic analysis

Based on the model shown in Fig. 3, the schematic diagrams of the displacement can be drawn for the rotating beam during its kinestate, as shown in Fig. 5.

The rotation angles of the rotating beam connected with the sliding part and the fixed block are expressed as follows:

$$\sin\theta_1 = \frac{y_2 - (y_1 - a\sin\theta)}{a}, \quad \cos\theta_1 = \frac{x_1 + a\cos\theta}{a}, \tag{5a}$$

$$\sin\theta_2 = \frac{a\sin\theta - y_2}{a}, \quad \cos\theta_2 = \frac{x_1 + a\cos\theta}{a}, \tag{5b}$$

where x_1 is the displacement of m_2 along the x-direction (equal to s), and y_2 is the displacement of m_2 along the y-direction.

The displacements during the movement of the energy harvester can be obtained with the trigonometric function relationship as follows:

$$\theta_2 = \theta_1, \quad y_1 = 2y_2, \quad x_1^2 + y_2^2 = 2a(y_2\sin\theta - x_1\cos\theta). \tag{6}$$

Figure 6 shows the force analysis of the energy harvester. The dynamic equations can be derived as follows:

$$\begin{cases} m_1\ddot{y}_1 = F - F_1\sin\theta_1, \quad (m_2+m_3)\ddot{y}_2 = F_1\sin\theta_1 - F_3\sin\theta_1, \\ (m_2+m_3)\ddot{x}_1 = F_1\cos\theta_1 + F_3\cos\theta_1 - kx_1. \end{cases} \tag{7}$$

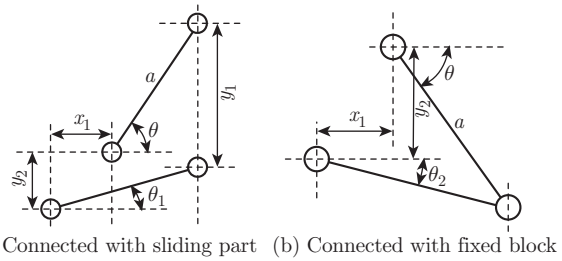

(a) Connected with sliding part (b) Connected with fixed block

Fig. 5 Schematic diagrams of displacement for rotating beam

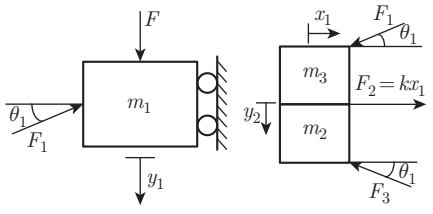

(a) m_1 (b) m_2 and m_3

Fig. 6 Force analysis of energy harvester

Combine Eq. (6) and Eq. (7). Then, the final forms of dynamic equations of the PF with the AF can be written as

$$\begin{cases} x_1^2 + y_2^2 = 2a(y_2\sin\theta - x_1\cos\theta), \\ (m_2+m_3)\ddot{x}_1 = (2F - (4m_1+m_2+m_3)\ddot{y}_2)\cot\theta_1 - kx_1. \end{cases} \tag{8}$$

In order to solve the dynamic equations conveniently, by considering $x_1^2 < y_2^2 \ll x_1 < y_2$, x_1^2 and y_2^2 in the formula are ignored.

The stiffness k is an important parameter that needs to be identified. Here, the finite element simulation is used to analyze the statics of the PF to get the stiffness. First, the strain energy distribution can be obtained as shown in Fig. 7 for the PF with different numbers of piezo-beams. Furthermore, the force-displacement curves are demonstrated in Fig. 8, where the stiffness can be easily obtained. It is clear that the stiffness is linear. Substitute the stiffness into Eq. (8). Then, the solutions to the dynamic equations are obtained and compared with the finite element simulation results, as shown in Fig. 9. It needs to be mentioned that the effect of damping is not considered in the simplified dynamic model, and the mechanical amplification factor will approach infinity at resonance. The solution result is not very accurate, but it is sufficient for the study on parameter characteristics.

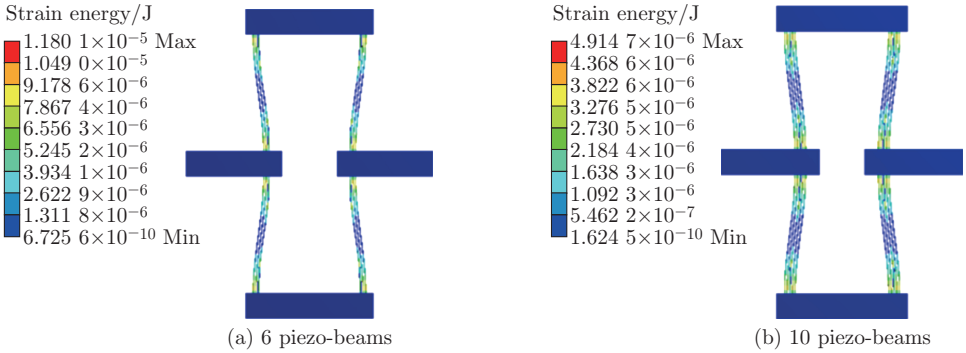

(a) 6 piezo-beams (b) 10 piezo-beams

Fig. 7 Strain energy distributions for PF with different numbers of piezo-beams (color online)

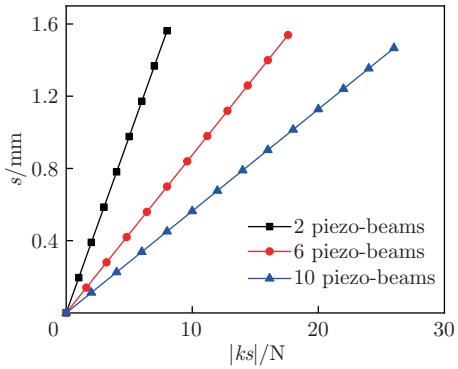

Fig. 8 Displacements of PF with different numbers of piezo-beams under static force (color online)

In order to facilitate the study on parameter characteristics, the initial parameters are set as follows: $m_1 = m_2 = m_3 = 0.1$ kg, $F = \sin(\omega t)$, $k = 1 \times 10^6$ N/m, $a = 0.03$ m, $\theta = 0.44$ rad. Based on the analysis of the influence of parameter characteristics on the amplitude-frequency response, it is shown that the first-order natural frequency of the PF with the AF has a positive correlation with k and θ, while a negative correlation with m_1. Under low-frequency non-resonant conditions, increasing k and m_1 or decreasing θ is beneficial to improving the mechanical amplification factor. Changing a will not affect the mechanical amplification factor.

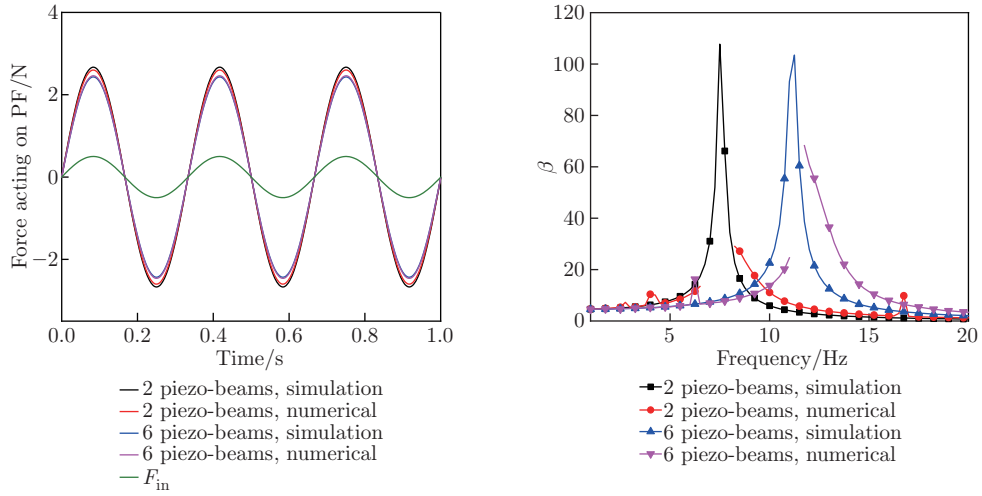

(a) Time-domain curves of force acting on PF at low-frequency vibration

(b) Frequency responses of mechanical amplification factor

Fig. 9 Numerical results compared with finite element simulation results for different numbers of piezo-beams (color online)

4 Energy harvesting performance

4.1 Stiffness analysis

Under strong excitations or impacts, the PF with the AF will loss the normal working ability as shown in Fig. 10(a). The structure will not automatically return to its normal state due to self-locking. Increasing the number of piezo-beams in the PF or adding springs (see Fig. 10(b)) can effectively avoid structural failure.

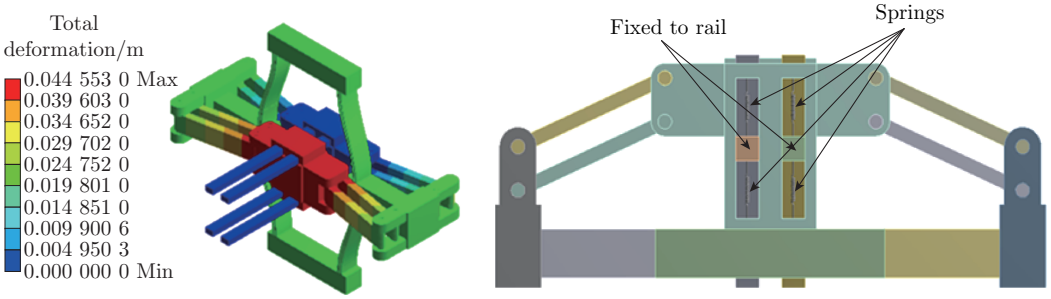

(a) Structural failure in three-dimensional mode

(b) Springs installed in PF with AF

Fig. 10 Structural failure of energy harvester and spring installation method (color online)

The finite element simulation is used to analyze the load capacity of the PF with the AF. It can be seen from Fig. 11 that, by increasing the number of piezo-beams in the PF or adding springs, the load capacity of the PF with the AF is improved. The stiffness of the PF with the AF is positively related to the number of piezo-beams on the PF. Furthermore, the overall stiffness of the additional springs is 8 N/mm.

The energy harvester deforms during the static state, and the energy input caused by static

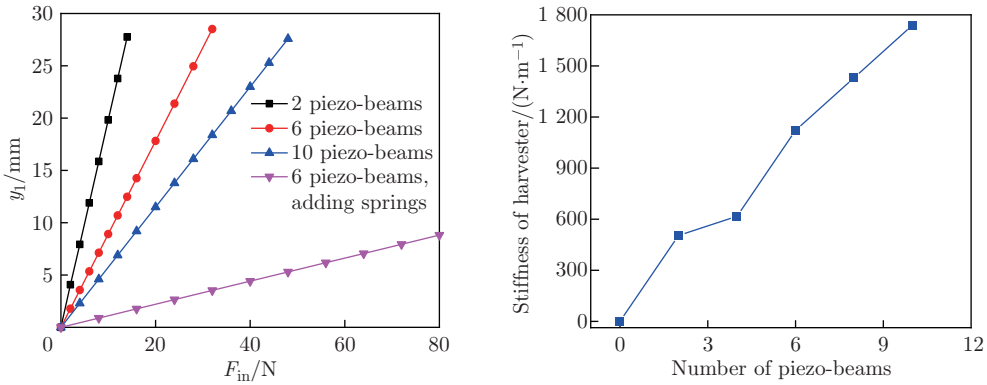

(a) Displacement of sliding pair under static force

(b) Stiffness of PF with AF with different numbers of piezo-beams

Fig. 11 Stiffness characteristic analysis of energy harvester (color online)

forces can be expressed as

$$W_{\text{in}} = F_{\text{in}} X, \tag{9}$$

where X denotes the displacement caused by static forces.

Since the energy harvesting of the piezoelectric sheet is related to the strain energy, the energy conversion efficiency (μ) is then defined as the ratio of the strain energy generated by piezoelectric sheets to the energy input (W_{in}). Apply the same external force (12 N) to the PF and the PF with the AF, respectively, to study the strain energy of piezoelectric sheets and the energy conversion efficiency. It can be seen from Table 2 that adding the AF to the PF has the same effect as increasing the strain energy of piezoelectric sheets, but the energy conversion efficiency remains unchanged due to the simultaneous increase in the energy input. Increasing the number of piezo-beams helps improve the energy conversion efficiency but reduces the strain energy of a single-beam piezoelectric sheet. Adding springs to the energy harvester will cause a significant decrease in the energy harvesting efficiency.

Table 2 Energy conversion efficiency of PF and PF with AF under the same force

Number of piezo-beams	W_{in} /J		Strain energy/J		μ/%		β
	PF	PF with AF	PF	PF with AF	PF	PF with AF	
2	0.099 99	0.507 44	0.016 20	0.084 80	16.2	16.7	5.235
6	0.044 77	0.228 44	0.007 88	0.039 98	17.6	17.5	5.074
10	0.028 88	0.147 11	0.005 46	0.028 10	18.9	19.1	5.147
6, adding springs	0.044 77	0.028 23	0.007 88	0.000 26	17.6	0.93	0.033

The following piezoelectric equations are used to obtain the voltage output of the energy harvester:

$$S_j = s_{ij}^{\text{E}} T_j + d_{ij} E_j, \quad D_i = d_{ij} T_j + \varepsilon_{ij}^{\text{T}} E_j. \tag{10}$$

Because the piezoelectric sheet is thin and mainly produces bending deformations, the piezoelectric effects of d_{31} are considered (the influence of d_{33} during bending is much smaller than that of d_{31}). By ignoring the influence of the inverse piezoelectric effect, the open-circuit voltage output of a single-beam piezoelectric sheet in the energy harvester is obtained, i.e.,

$$v_0 = A_3 \frac{d_{31} T_1}{C_3}, \tag{11a}$$

where T_1 represents the stress of the piezoelectric sheet, A_3 represents the surface area of the piezoelectric sheet, and C_3 represents the capacitance of the piezoelectric sheet, which can be written as

$$C_3 = \frac{A_3 \varepsilon_{33}^{\mathrm{T}}}{d_3}, \tag{11b}$$

where d_3 represents the thickness of the piezoelectric sheet.

The rotation and structural damping coefficients are 0.05 and 0.02, respectively. Finite element simulation is used to analyze the harmonic response. As shown in Fig. 12, the frequency responses of the amplitude of open-circuit voltage for a single-beam piezoelectric sheet in the energy harvester under the given sinusoidal excitation of 0.5 N are obtained in conjunction with Eqs. (11a) and (11b). From Fig. 12, the addition of the AF can reduce the natural frequency of the energy harvester and help increase the voltage output under low-frequency vibration. The PF with the AF can resonate under low-frequency vibration conditions.

Under the given sinusoidal acceleration excitation of 0.5 m/s^2, the influence of the number of piezo-beam and additional spring on the open-circuit voltage output of the PF with the AF is studied, as shown in Fig. 13. It shows that an increase in the number of piezo-beams will increase the first-order natural frequency of the energy harvester. For low-frequency non-resonant conditions, an increase in the number of piezo-beams causes a decrease in the open-circuit voltage output of a single-beam piezoelectric sheet. Adding a spring will cause the decrease in the open-circuit voltage output of the energy harvester. In addition, there will be no structural failure within the frequency range.

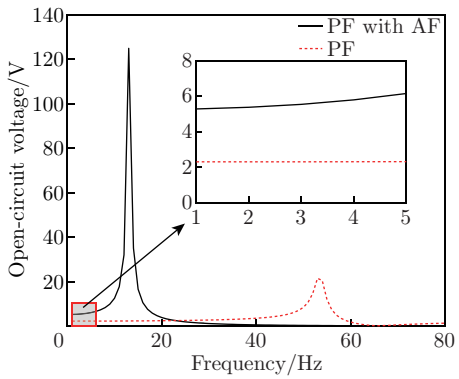

Fig. 12 Frequency responses of open-circuit voltage of PF and PF with AF (color online)

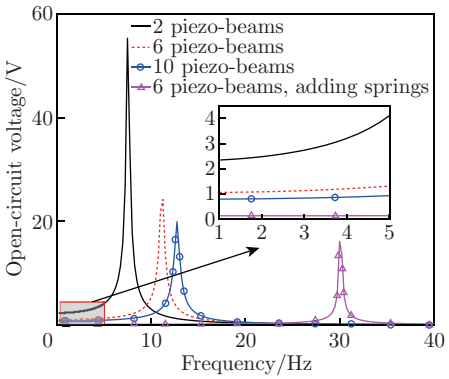

Fig. 13 Frequency responses of open-circuit voltage of energy harvester with springs for different numbers of piezo-beams (color online)

4.2 Power output

The power output of the energy harvester is analyzed under the condition of external load resistance. Ignore the influence of internal resistance, and consider that each piezoelectric sheet is connected in parallel or in series.

$$I_z(t) = \sum_{i=1}^{N} I_i(t) = \frac{v(t)}{R} \ \text{ in parallel}, \quad V_z(t) = \sum_{i=1}^{N} V_i(t) = i(t)R \ \text{ in series}, \tag{12}$$

where I_z is the total current output for the piezoelectric sheet connected in parallel, V_z is the total voltage output for the piezoelectric sheet connected in series, N represents the number of

piezoelectric sheets, R represents the load resistance of the energy harvester, v represents the voltage of parallel circuit, and i represents the current of series circuit.

Consider that the size and stress distribution of each piezoelectric sheet are exactly the same. Then, Eq. (12) can be simplified as follows:

$$NA_3\frac{\mathrm{d}}{\mathrm{d}t}D_3(t)=\frac{v(t)}{R}\ \text{ in parallel},\quad NE_3(t)d_1=i(t)R\ \text{ in series},\tag{13}$$

where D_3 is the electric displacement of each piezoelectric sheet, and E_3 is the electric field of each piezoelectric sheet.

Combine Eq. (13) with Eq. (11) to obtain the voltage output, i.e.,

$$C_{\mathrm{p}}\dot{v}(t)+\frac{v(t)}{R}=Nd_{31}\dot{T}_1(t)A_3,\quad C_{\mathrm{s}}\dot{v}(t)+\frac{v(t)}{R}=d_{31}\dot{T}_1(t)A_3,\tag{14}$$

where C_{p} is the equivalent capacitance for the piezoelectric sheet connected in parallel, and C_{s} is the equivalent capacitance for the piezoelectric sheet connected in series, i.e.,

$$C_{\mathrm{p}}=\frac{NA_3\varepsilon_{33}^{\mathrm{T}}}{d_3},\quad C_{\mathrm{s}}=\frac{A_3\varepsilon_{33}^{\mathrm{T}}}{Nd_3}.$$

Consider that the stress is sinusoidal, and the numerical solution to Eq. (12) is obtained to get the maximum instantaneous power output of the energy harvester, i.e.,

$$T_1(t)=P_1\sin(\omega t),\quad p=\frac{v^2}{R},\tag{15}$$

where P_1 represents the amplitude of stress, p is the maximum instantaneous power output, and v is the amplitude of voltage output.

Take the PF with the AF (6 piezo-beams) to study the effects of load resistance and frequency on the maximum instantaneous power output of the energy harvester, as shown in Fig. 14. Under the condition of 0.5 m/s^2 sinusoidal acceleration excitation (5 Hz), the impedance matching research results show that the matching resistance required in parallel is much lower than that in series. Without the consideration of the internal resistance, the maximum instantaneous powers of the two wiring methods under the matched impedance are

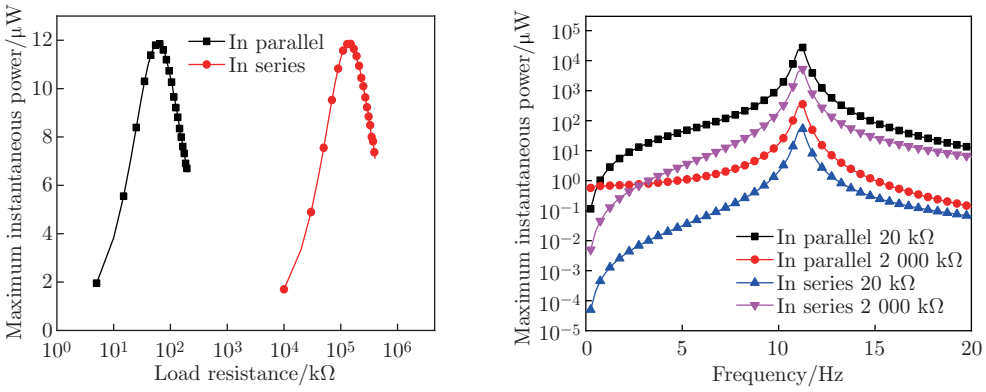

(a) Impedance matching

(b) Frequency responses of maximum instantaneous power

Fig. 14 Effects of load resistance and frequency on the maximum instantaneous power output of energy harvester for piezoelectric sheets connected in parallel and in series (color online)

the same. It can be seen from Fig. 14 that it is more advantageous to use the parallel connection pattern under the condition of low-load resistance.

As shown in Fig. 15, the influence of the number of piezo-beams on the power output is studied under the condition of piezoelectric sheets connected in parallel (load resistance 20 kΩ). Designing the structure of the PF with the AF in combination with specific electrical appliances can maximize the output power.

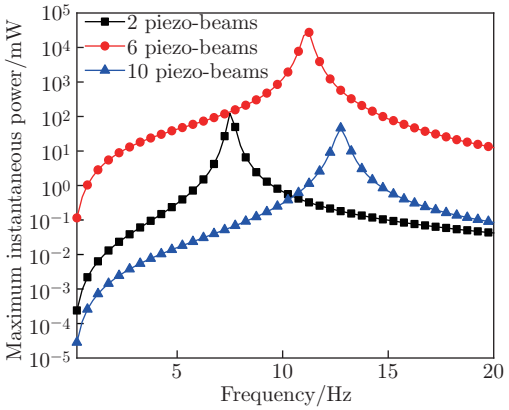

Fig. 15 Power output of energy harvesters with different numbers of piezo-beams (color online)

In short, the factors including the two connection patterns of the piezoelectric sheet, frequency and amplitude of vibration, structure parameters of energy harvesters, and impedance of load electrical appliances can affect the power of the energy harvester in the closed circuit. It is simple and effective to use the open-circuit voltage output of a single-beam piezoelectric sheet to measure the energy harvesting efficiency of the PF with the AF under the condition of no-load electrical appliances.

4.3 Comparison of results

To demonstrate the advantages of the proposed energy harvester including the PF and the AF, the results are compared with those of a conventional harvester made by only a cantilever piezoelectric beam. Of course, the excitation condition, the laying area, the materials, and the thickness of the piezoelectric sheet are guaranteed to be the same for both two kinds of energy harvesters.

As shown in Fig. 16, adding the mass to the end of the piezoelectric cantilever reduces the natural frequency of the system, but increases the inertial force generated due to acceleration excitation. Piezoelectric sheets on the cantilever beam are laid from the fixed end because the strain is mainly distributed here. The length, thickness, and material of cantilever beams and piezo-beams are the same.

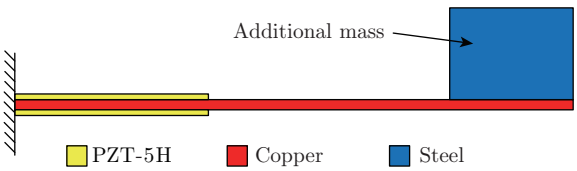

Fig. 16 Schematic diagram of piezoelectric cantilever beam (color online)

By considering the low-frequency non-resonant vibration conditions, Fig. 17 demonstrates that the voltage output of the piezoelectric cantilever beam increases with the increase in the

additional mass, but it is difficult to exceed the voltage output of the PF with the AF. When the piezoelectric cantilever beam resonates, its open-circuit voltage output may be higher than that of the PF with the AF. Due to the difference in usage scenarios and excitation conditions, it cannot be concluded that the energy harvesting effect of the PF with the AF must be higher than that of the piezoelectric cantilever beam. Compared with piezoelectric cantilever beams, the PF with the AF is more integrated and more suitable for collecting vibration energy generated by a single excitation source.

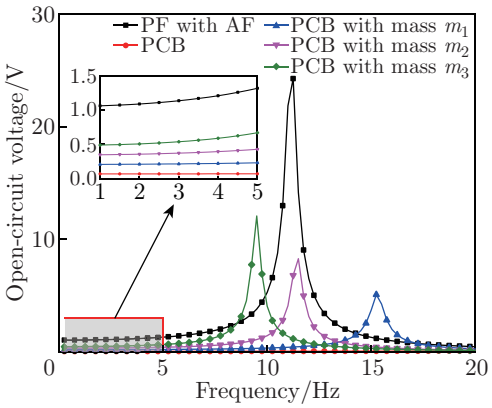

Fig. 17 Energy harvesting effects of PF with AF under acceleration excitation, where PCB denotes piezoelectric cantilever beam (color online)

4.4 Beam optimization

As seen from Fig. 18, the stress for the variable cross-section piezoelectric sheet is more uniformly-distributed than that for the equal cross-section one. The harvesting performance of the VEH with varying cross-section piezoelectric beams has been studied, and its advantages are verified[37–39]. In this paper, a variable cross-section piezoelectric beam is designed to improve the energy conversion efficiency, as shown in Fig. 19. The variable cross-section coefficient is defined as $\alpha = h/H$. The ratio of the laying area of the piezoelectric sheet λ to the area of the varying cross-section beam ζ is expressed as

$$\gamma = \frac{\lambda}{\zeta} = \frac{2(H + h_1)l}{(H + h)L_1}. \tag{16}$$

The effect of the variable cross-section piezo-beam on the energy conversion efficiency of the energy harvester is studied, as shown in Fig. 20. The energy conversion efficiency of the energy

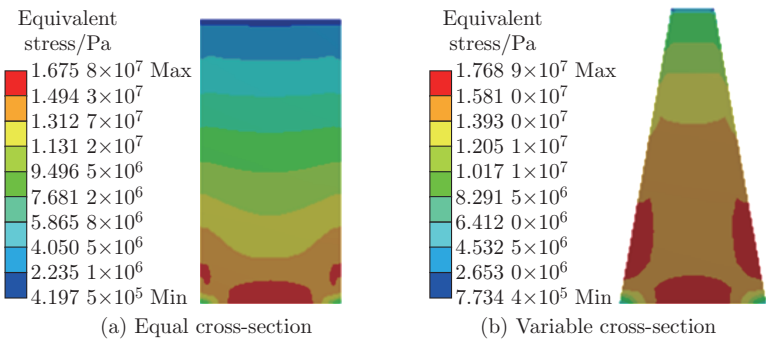

Fig. 18 Stress distributions of piezoelectric sheet (color online)

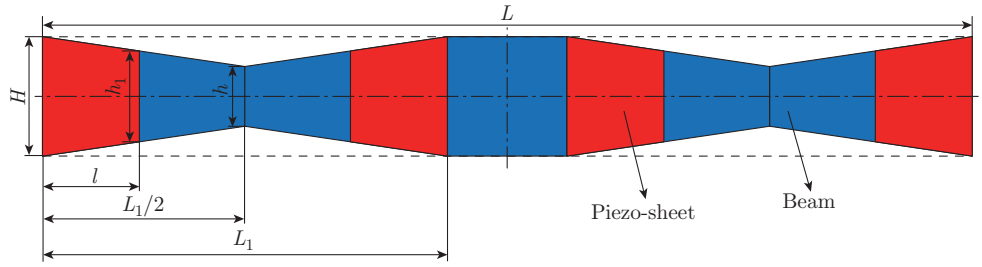

Fig. 19 Structure of varying cross-section beam (color online)

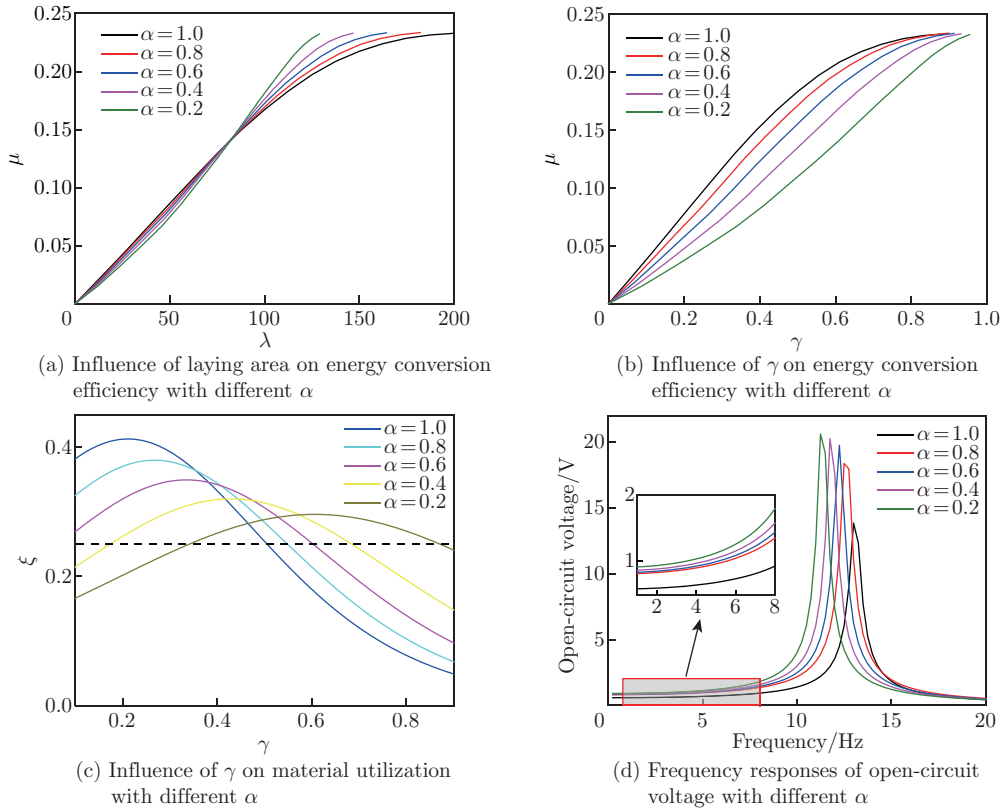

(a) Influence of laying area on energy conversion efficiency with different α

(b) Influence of γ on energy conversion efficiency with different α

(c) Influence of γ on material utilization with different α

(d) Frequency responses of open-circuit voltage with different α

Fig. 20 Effects of variable cross-section beams on energy harvesting with different α (color online)

harvester gradually increases with the increase in the laying area of the piezoelectric sheet. Under the condition of large laying areas, the variable cross-section coefficient is inversely related to the energy harvesting efficiency. The rate at which the energy conversion efficiency increases with γ is defined as the material utilization rate, expressed as $\xi = \frac{\mathrm{d}\mu}{\mathrm{d}\gamma}$. The utilization rate of piezoelectric materials shows a trend of increasing first and then decreasing with the increase in the laying area.

Table 3 shows the energy conversion efficiency when the material utilization rate is 0.25. The use of varying cross-section piezo-beams is conducive to saving piezoelectric materials. Moreover, for the energy harvesters with the same laying area but with different varying cross-section coefficients, the voltage output is compared, as shown in Fig. 20(d). It is clear that the lower the varying cross-section coefficient, the better the energy harvesting performance.

Table 3 Energy conversion efficiency of varying cross-section piezoelectric sheet for $\xi = 0.25$

α	λ/mm^2	γ	$\mu/\%$
1.0	113.88	0.506 14	18.51
0.8	111.40	0.550 13	18.55
0.6	109.20	0.606 67	18.65
0.4	108.17	0.686 82	19.00
0.2	117.69	0.871 75	21.59

5 Conclusions

In this paper, an original design of an integrated architecture with the PF and the AF for the VEH is proposed and analyzed. The dynamic model of the proposed harvester is established to study the influence of key parameters on the mechanical amplification factor. It is concluded that the reasonable structural design of the AF can simultaneously increase the external force acting on the PF and prevent the piezoelectric layer from being damaged. It can also reduce the natural frequency of the energy harvester and increase the mechanical amplification factor during the low-frequency vibration, if the parameters including the stiffness of the PF, the length of beams, the structural angle, and the mass of sliding parts, are chosen properly.

The finite element simulation is also used to study the harvesting characteristics of the energy harvester. Under the condition that the energy harvester is connected with a low resistance, the piezoelectric sheets connected in parallel have a higher power output. The modal analysis results show that the addition of the AF can reduce the first-order natural frequency of the energy harvester. The number of piezoelectric sheets on the PF with the AF (6 piezo-beams) is equivalent to that on four piezoelectric cantilever beams (24 piezo-beams). Compared with piezoelectric cantilever beams, the PF with the AF is more suitable for collecting vibration energy generated by the same excitation source. When piezoelectric sheets are laid over a large area, the use of variable cross-section beams can improve the utilization of piezoelectric materials.

The energy harvester designed in this paper can be used to collect vibration energy generated under various environmental conditions such as road, bridge, and motor rotation. The PF with the AF will have a higher energy output when the system resonates. By using the method of collision (removing the spring in Fig. 10(b)) and bistable structure design (the self-locking phenomenon in Fig. 10(a) is essentially that the system jumps to another steady state under a large excitation force), the resonance bandwidth of the energy harvester can be broadened. The following research will mainly focus on the practical application of the energy harvester and the widening of the working bandwidth.

Open Access This article is licensed under a Creative Commons Attribution 4.0 International License, which permits use, sharing, adaptation, distribution and reproduction in any medium or format, as long as you give appropriate credit to the original author(s) and the source, provide a link to the Creative Commons licence, and indicate if changes were made. To view a copy of this licence, visit http://creativecommons.org/licenses/by/4.0/.

References

[1] ROUNDY, S., WRIGHT, P. K., and RABAEY, J. A study of low level vibrations as a power source for wireless sensor nodes. *Computer Communications*, **26**(11), 1131–1144 (2003)

[2] DAQAQ, M. F., MASANA, R., ERTURK, A., and QUINN, D. D. On the role of nonlinearities in vibratory energy harvesting: a critical review and discussion. *Applied Mechanics Reviews*, **66**(4), 045501 (2014)

[3] ZOU, H. X., ZHAO, L. C., GAO, Q. H., ZUO, L., LIU, F. R., TAN, T., WEI, K. X., and ZHANG, W. M. Mechanical modulations for enhancing energy harvesting: principles, methods and applications. *Applied Energy*, **255**, 113871 (2019)

[4] WANG, J., GENG, L., DING, L., ZHU, H., and YURCHENKO, D. The state-of-the-art review on energy harvesting from flow-induced vibrations. *Applied Energy*, **267**, 114902 (2020)

[5] LALLART, M., WANG, L., and PETIT, L. Enhancement of electrostatic energy harvesting using self-similar capacitor patterns. *Journal of Intelligent Material Systems and Structures*, **27**(17), 2385–2394 (2016)

[6] PEREZ, M., BOISSEAU, S., GASNIER, P., WILLEMIN, J., GEISLER, M., and REBOUD, J. L. A cm scale electret-based electrostatic wind turbine for low-speed energy harvesting applications. *Smart Materials and Structures*, **25**(4), 045015 (2016)

[7] ZHANG, Y., WANG, T., ZHANG, A., PENG, Z., LUO, D., CHEN, R., and WANG, F. Electrostatic energy harvesting device with dual resonant structure for wideband random vibration sources at low frequency. *Review of Scientific Instruments*, **87**(12), 125001 (2016)

[8] LI, X., ZHANG, Y., DING, H., and CHEN, L. Integration of a nonlinear energy sink and a piezoelectric energy harvester. *Applied Mathematics and Mechanics* (*English Edition*), **38**(7), 1019–1030 (2017) https://doi.org/10.1007/s10483-017-2220-6

[9] GUO, X. Y., JIANG, P., ZHANG, W., YANG, J., KITIPORNCHAI, S., and SUN, L. Nonlinear dynamic analysis of composite piezoelectric plates with graphene skin. *Composite Structures*, **206**, 839–852 (2018)

[10] CAO, D., GUO, X., and HU, W. A novel low-frequency broadband piezoelectric energy harvester combined with a negative stiffness vibration isolator. *Journal of Intelligent Material Systems and Structures*, **30**(7), 1105–1114 (2019)

[11] LU, Z. Q., DING, H., and CHEN, L. Q. Resonance response interaction without internal resonance in vibratory energy harvesting. *Mechanical Systems and Signal Processing*, **121**, 767–776 (2019)

[12] ZHOU, S. X., CAO, J. Y., INMAN, D. J., LIN, J., LIU, S. S., and WANG, Z. Z. Broadband tristable energy harvester: modeling and experiment verification. *Applied Energy*, **133**, 33–39 (2014)

[13] LIU, D., XU, Y., and LI, J. L. Randomly-disordered-periodic-induced chaos in a piezoelectric vibration energy harvester system with fractional-order physical properties. *Journal of Sound and Vibration*, **399**, 182–196 (2017)

[14] LAI, S. K., WANG, C., and ZHANG, L. H. A nonlinear multi-stable piezomagnetoelastic harvester array for low-intensity, low-frequency, and broadband vibrations. *Mechanical Systems and Signal Processing*, **122**, 87–102 (2019)

[15] ZHANG, L., XU, X., HAN, Q., QIN, Z., and CHU, F. Energy harvesting of beam vibration based on piezoelectric stacks. *Smart Materials and Structures*, **28**(12), 125020 (2019)

[16] MORGADO, M. L., MORGADO, L. F., SILVA, N., and MORAIS, R. Mathematical modelling of cylindrical electromagnetic vibration energy harvesters. *International Journal of Computer Mathematics*, **92**(1), 101–109 (2014)

[17] MOSS, S. D., PAYNE, O. R., HART, G. A., and UNG, C. Scaling and power density metrics of electromagnetic vibration energy harvesting devices. *Smart Materials and Structures*, **24**(2), 023001 (2015)

[18] WANG, W., CAO, J., ZHANG, N., LIN, J., and LIAO, W. H. Magnetic-spring based energy harvesting from human motions: design, modeling and experiments. *Energy Conversion and Management*, **132**, 189–197 (2017)

[19] DENG, Q., KAMMOUN, M., ERTURK, A., and SHARMA, P. Nanoscale flexoelectric energy harvesting. *International Journal of Solids and Structures*, **51**(18), 3218–3225 (2014)

[20] LIANG, X., HU, S., and SHEN, S. Nanoscale mechanical energy harvesting using piezoelectricity and flexoelectricity. *Smart Materials and Structures*, **26**(3), 035050 (2017)

[21] ANTON, S. R., FARINHOLT, K. M., and ERTURK, A. Piezoelectret foam-based vibration energy harvesting. *Journal of Intelligent Material Systems & Structures*, **25**(14), 1681–1692 (2014)

[22] ZHANG, X., PONDROM, P., SESSLER, G. M., and MA, X. Ferroelectret nanogenerator with large transverse piezoelectric activity. *Nano Energy*, **50**, 52–61 (2018)

[23] KIM, H., PRIYA, S., and UCHINO, K. Modeling of piezoelectric energy harvesting using cymbal transducers. *Japanese Journal of Applied Physics*, **45**(7), 5836–5840 (2006)

[24] KIM, H. W., BATRA, A., PRIYA, S., UCHINO, K., MARKLEY, D., NEWNHAM, R. E., and HOFMANN, H. F. Energy harvesting using a piezoelectric "cymbal" transducer in dynamic environment. *Japanese Journal of Applied Physics*, **43**(9A), 6178–6183 (2004)

[25] LI, X., GUO, M., and DONG, S. A flex-compressive-mode piezoelectric transducer for mechanical vibration/strain energy harvesting. *IEEE Transactions on Ultrasonics, Ferroelectrics, and Frequency Control*, **58**(4), 698–703 (2011)

[26] MO, C., ARNOLD, D., KINSEL, W. C., and CLARK, W. W. Modeling and experimental validation of unimorph piezoelectric cymbal design in energy harvesting. *Journal of Intelligent Material Systems and Structures*, **24**(7), 828–836 (2012)

[27] MOURE, A., IZQUIERDO RODRÍGUEZ, M. A., HERNÁNDEZ RUEDA, S., GONZALO, A., RUBIO-MARCOS, F., URQUIZA CUADROS, D., PÉREZ-LEPE, A., and FERNÁNDEZ, J. F. Feasible integration in asphalt of piezoelectric cymbals for vibration energy harvesting. *Energy Conversion and Management*, **112**, 246–253 (2016)

[28] WANG, X., SHI, Z., WANG, J., and XIANG, H. A stack-based flex-compressive piezoelectric energy harvesting cell for large quasi-static loads. *Smart Materials and Structures*, **25**(5), 055005 (2016)

[29] ZHAO, H., YU, J., and LING, J. Finite element analysis of cymbal piezoelectric transducers for harvesting energy from asphalt pavement. *Journal of the Ceramic Society of Japan*, **118**(1382), 909–915 (2010)

[30] LING, M., CAO, J., JIANG, Z., and LIN, J. Theoretical modeling of attenuated displacement amplification for multistage compliant mechanism and its application. *Sensors and Actuators A: Physical*, **249**, 15–22 (2016)

[31] CAO, J., LING, M., INMAN, D. J., and LIN, J. Generalized constitutive equations for piezo-actuated compliant mechanism. *Smart Materials and Structures*, **25**(9), 095005 (2016)

[32] EVANS, M., TANG, L., and AW, K. C. Modelling and optimisation of a force amplification energy harvester. *Journal of Intelligent Material Systems and Structures*, **29**(9), 1941–1952 (2018)

[33] WEN, S. and XU, Q. Design of a novel piezoelectric energy harvester based on integrated multistage force amplification frame. *IEEE/ASME Transactions on Mechatronics*, **24**(3), 1228–1237 (2019)

[34] WEN, S., XU, Q., and ZI, B. Design of a new piezoelectric energy harvester based on compound two-stage force amplification frame. *IEEE Sensors Journal*, **18**(10), 3989–4000 (2018)

[35] WEN, S. H., WU, Z. H., and XU, Q. S. Design of a novel two-directional piezoelectric energy harvester with permanent magnets and multistage force amplifier. *IEEE Transactions on Ultrasonics Ferroelectrics and Frequency Control*, **67**(4), 840–849 (2020)

[36] CAO, D. X., DUAN, X. J., GUO, X. Y., and LAI, S. K. Design and performance enhancement of a force-amplified piezoelectric stack energy harvester under pressure fluctuations in hydraulic pipeline systems. *Sensors and Actuators A: Physical*, **309**, 112031 (2020)

[37] CAO, D. X., DING, X. D., GUO, X. Y., and YAO, M. H. Design, simulation and experiment for a vortex-induced vibration energy harvester for low-velocity water flow. *International Journal of Precision Engineering and Manufacturing — Green Technology* (2020) https://doi.org/10.1007/s40684-020-00265-9

[38] BEN AYED, S., ABDELKEFI, A., NAJAR, F., and HAJJ, M. R. Design and performance of variable-shaped piezoelectric energy harvesters. *Intelligent Material Systems and Structures*, **25**(2), 174–186 (2014)

[39] MUTHALIF, A. G. A. and NORDIN, N. H. D. Optimal piezoelectric beam shape for single and broadband vibration energy harvesting: modeling, simulation and experimental results. *Mechanical Systems and Signal Processing*, **54-55**, 417–426 (2015)